

1 **Topography dominates the hemispheric asymmetry of**
2 **Stratospheric Sudden Warmings**

3 **Siming Liu¹, Tiffany Shaw¹, Chaim I. Garfinkel²**

4 ¹Department of the Geophysical Sciences, The University of Chicago, Chicago, IL

5 ²Fredy and Nadine Herrmann Institute of Earth Sciences, The Hebrew University of Jerusalem,
6 Jerusalem, Israel

7 **Key Points:**

- 8 • Climate model simulations are used to quantify the impact of topography and
9 ocean circulation on stratospheric sudden warmings.
10 • Topography is found to play a dominant role in shaping the hemispheric
11 asymmetry of SSWs through its control on eddy heat flux.
12 • Topography amplifies eddy heat flux by increasing the amplitude of eddy
13 meridional wind and temperature while decreasing their phase difference.

Corresponding author: Siming Liu, smliu01@uchicago.edu

Abstract

Stratospheric Sudden Warmings (SSWs) predominantly occur in the Northern Hemisphere with only 1 major event recorded in the Southern Hemisphere in the satellite era. Investigating factors that contribute to this asymmetry can help to reveal the cause of SSWs and lead to improved forecasts. Here we use climate model simulations to investigate the impact of boundary conditions (topography and ocean circulation) on the asymmetry. Flattening topography eliminates Northern Hemisphere SSWs, while removing the ocean meridional overturning circulation reduces their frequency by half. The SSW response to boundary conditions is controlled by the decrease in hemispheric asymmetry of eddy heat flux. The reduction is driven by a decrease in amplitude of both eddy meridional wind and eddy temperature, as well as an increase in the difference between their phases. The results suggest boundary conditions play an important role in shaping SSWs, especially topographic forcing, but that the boundary condition interactions are nonlinear.

Plain Language Summary

SSWs are powerful events that affect surface weather and climate. They mostly happen in the Northern Hemisphere, with very few occurring in the Southern Hemisphere. Understanding why this happens is important. Using climate model simulations, we quantify how boundary conditions, such as topography and ocean circulation, affect SSWs. The results suggest topography is the primary factor influencing the difference between hemispheres in SSWs. Topography is shown to control how much heat is transferred poleward by deviations from the zonal mean, which are known to drive SSWs. More specifically, flattening topography leads to changes in the wave phase and amplitude of meridional wind and temperature, which in turn causes a decrease in poleward eddy heat flux.

1 Introduction

Stratospheric Sudden Warmings (SSWs) represent dramatic and abrupt disruptions in the winter stratosphere, characterized by a rapid increase in temperature and a decrease in the zonal-mean zonal wind in the polar vortex region (Butler et al., 2015; Baldwin et al., 2021). SSWs impact weather and climate in the Northern Hemisphere (NH) (Baldwin & Dunkerton, 1999) and Southern Hemisphere (SH) (Thompson et al., 2005), by shifting jet streams and storm tracks (Baldwin & Dunkerton, 2001; Afargan-Gerstman & Domeisen, 2020), inducing precipitation and temperature anomalies (Lehtonen & Karpechko, 2016; Lim et al., 2019). Additionally, for the SH, it suppresses strong heterogeneous ozone depletion, consequently impeding the formation of the ozone hole (Varotsos, 2002).

A notable feature of SSWs is the distinct hemispheric asymmetry in their occurrence between the Northern and Southern Hemispheres (Krüger et al., 2005). The primary focus of SSWs has been on the NH, which occur roughly every 2 years (Baldwin et al., 2021). In contrast, only one major SSW in the Southern Hemisphere (SH) took place in September 2002 (Allen et al., 2003; Simmons et al., 2005; Allen et al., 2006), and a minor one occurred in September 2019 (Hendon et al., 2019; Yamazaki et al., 2020; Rao et al., 2020).

One of the primary factors contributing to SSWs is the breaking of planetary-scale waves that propagate upwards from the troposphere (Matsuno, 1971), an important source of stratospheric variability (Polvani & Waugh, 2004; Cohen & Jones, 2011; Shaw & Perlwitz, 2013, 2014; Sjöberg & Birner, 2012, 2014; Dunn-Sigouin & Shaw, 2015, 2018, 2020). It is expected that weaker winter stratospheric variability and much fewer SSWs in the SH are due to weaker tropospheric wave driving (Plumb, 1989). Stationary planetary waves in the troposphere can be triggered by various bottom boundary conditions (Held et al., 2002; Garfinkel et al., 2020), including large-scale topography (Charney & Eliassen, 1949), surface thermal forcing such as land-sea contrasts (Smagorinsky, 1953) and asymmetric

63 surface energy fluxes (Shaw et al., 2022), and the nonlinear interactions of synoptic-scale
64 eddies (Scinocca & Haynes, 1998).

65 Previous research has primarily focused on investigating the impact of idealized
66 topography on stratospheric variability. Dry dynamical core models show the seasonal and
67 interannual variability of extratropical stratospheric circulation depends on the amplitude
68 of idealized topography, and hence on topographically forced stationary waves (Taguchi &
69 Yoden, 2002; Gerber & Polvani, 2009; Sheshadri et al., 2015; Lindgren et al., 2018; Dunn-
70 Sigouin & Shaw, 2018, 2020). These studies have shown that increasing the amplitude of
71 idealized wave-2 topography leads to the stratosphere entering a regime in which SSWs
72 take place. Specifically, the small amplitude of topography corresponds to the SH where
73 the polar night jet is strong and stratospheric variability is small while for large amplitude
74 topography corresponding to the NH stratospheric variability is large. However, only a
75 limited number of studies (e.g., Garfinkel et al., 2020) have examined the impact of realistic
76 topography with land and compared the relative importance of different factors triggering
77 tropospheric planetary waves that lead to SSWs. This research gap signals the need for a
78 more comprehensive understanding of the various forcings contributing to the occurrence of
79 SSWs.

80 Here we seek to address the following questions: (a) What are the relative contributions
81 of boundary conditions, including topography and the ocean meridional overturning
82 circulation, to the hemispheric asymmetry of SSWs? (b) Through what mechanisms do
83 boundary conditions affect stratospheric variability? Our approach to answering these
84 questions involves examining SSWs in climate model simulations with modified surface
85 (land and ocean) boundary conditions.

86 **2 Data and Methods**

87 **2.1 Climate Model Simulations**

88 We make use of the ECHAM6 slab-ocean atmosphere general circulation model
89 simulations previously reported by Shaw et al. (2022). The model incorporates a
90 realistic land surface featuring topography, a 50 meter mixed layer ocean depth, and has
91 prescribed monthly varying observationally-derived surface energy fluxes over the ocean.
92 The observationally-derived surface energy fluxes are quantified by the difference of NASA
93 CERES TOA radiative flux and the atmospheric energy flux divergence derived from ERA-
94 Interim reanalysis data (Frierson et al., 2013; Shaw et al., 2022). Similar results are found
95 when the surface energy fluxes are q-flux derived from an prescribed sea surface temperature
96 simulation.

97 The impact of boundary conditions on the hemispheric asymmetry of SSWs,
98 is quantified by comparing 60-year simulations with realistic boundary conditions to
99 simulations with flattened topography and symmetric surface energy fluxes. As discussed
100 in Shaw et al. (2022), the flattened topography experiment involves setting the surface
101 geopotential and mean orography to zero in the surface boundary condition input file.
102 The symmetrized surface energy flux experiment involves setting the surface energy flux
103 at each latitude to the average of the surface energy flux (over the ocean) for the Northern
104 Hemisphere and Southern Hemispheres. Symmetrizing the surface energy fluxes removes
105 the ocean meridional overturning circulation (Frierson et al., 2013) and east-west sea-surface
106 temperature gradients.

107 **2.2 Reanalysis**

108 The ERA5 reanalysis (Hersbach et al., 2020) from 1958-2022 is used in this study. We
109 used daily zonal and meridional wind and temperature to evaluate the model's ability to
110 simulate a reasonable frequency of SSWs and eddy meridional heat flux.

2.3 SSW and eddy heat flux definitions

The identification of a major SSW in both hemispheres follows the method in Charlton and Polvani (2007). A major SSW is identified when the zonal mean westerlies at 60°N/60°S and 10 hPa change to easterlies during winter (November-March for the Northern Hemisphere, May-September for the Southern Hemisphere) and lasts for at least 3 days. The date of the wind reversal is designated as the onset date. Subsequent SSW events are not considered if they occur within 20 days following the most recent onset date. Events where zonal-mean easterlies fail to revert to westerlies before April are also excluded.

We calculate the monthly mean meridional eddy heat flux $\overline{v^*T^*}$ at 100 hPa to quantify the wave activity entering the stratosphere (Polvani & Waugh, 2004). Here, v and T are the meridional wind and temperature, respectively, while the overline and asterisk denote the monthly mean and deviations from the zonal mean. Additionally, v and T at 60°N and 100 hPa are decomposed into different wavenumbers. The amplitude and phase for each wave component are calculated following Watt-Meyer and Kushner (2018).

3 Results

3.1 The evaluation of the climate model

In ERA5, the frequency of SSWs per year (f_{SSW}) in the NH is approximately 0.61/year while there is only 1 major SSW in the SH, consistent with previous studies (Butler et al., 2015; Baldwin et al., 2021). The model forced with realistic boundary conditions, including observationally derived climatological surface energy fluxes, hereafter referred to as ALL, reproduces the observed f_{SSW} in the NH (Table 1 ALL), outperforming most CMIP5/6 simulations (Rao & Garfinkel, 2021). Additionally, it accurately simulates the hemispheric asymmetry in f_{SSW} , as the model simulation does not produce any SSWs in the Southern Hemisphere.

Table 1. Frequency of SSW (f_{SSW}) in Northern and Southern Hemisphere in ERA5 reanalysis (1958-2022) and in the climate model simulations forced with realistic boundary conditions, including observationally derived climatological surface energy fluxes (ALL). Frequency of SSW is also shown for simulations with perturbed boundary conditions: flattened topography (FLAT), symmetrized surface energy fluxes (SYMS), and flattened topography and symmetrized surface energy fluxes (F+S).

	NH	SH
ERA5	40/65	1/65
ALL	40/60	0/60
FLAT	1/60	0/60
SYMS	22/60	0/60
F+S	0/60	0/60

Our simulations do not simulate any SSWs in the SH. At first glance this might seem like a model bias, however we consider this outcome to be not unexpected. Jucker and Reichler (2023) demonstrate the occurrence of 161 SSWs in the SH through a 9990-year coupled climate model simulation, with a frequency of one event every 62 years. Hence, it is plausible for no SSWs to manifest within a 60-year simulation period.

140 To further assess the model’s capability in simulating stratospheric variability, Fig. 1
 141 illustrates the monthly distribution of SSW frequency in the NH. In contrast to a common
 142 bias observed in CMIP5/6 simulations, where SSWs are most frequent in late winter
 143 (February-March) rather than midwinter (January-February) (Wu & Reichler, 2020; Rao &
 144 Garfinkel, 2021), the model’s climatology simulation (ALL) exhibits SSWs predominantly
 145 in midwinter.

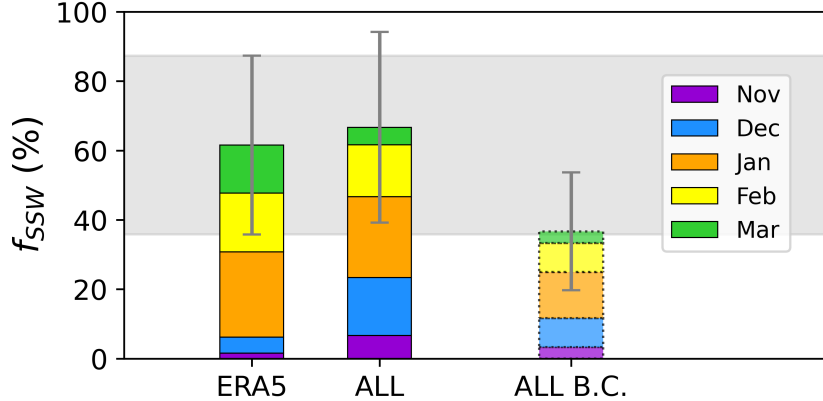


Figure 1. Monthly Distribution of the SSW frequency (f_{SSW}) in the NH of ERA5 (1958–2022) and climate model simulations (ALL). The third column (ALL B.C.) is the bias corrected ALL simulation where the daily zonal-mean zonal wind climatology at 10 hPa and 60°N (U_{1060}) is corrected by replacing it with ERA5. The gray shading represents the 95% confidence interval of ERA5 and the gray whisker on each bar represents the 95% confidence interval of each simulation.

146 The simulated f_{SSW} can be affected by biases in the climatological mean state of the
 147 polar vortex (Scaife et al., 2010). When the ALL daily zonal-mean zonal wind climatology
 148 at 10 hPa and 60°N is replaced by that from ERA5 f_{SSW} decreases (Fig. 1, ALL B.C.),
 149 indicating an underestimation of U_{1060} (Fig. S1a,m). Despite the presence of a bias in
 150 the magnitude of the climatological zonal mean zonal wind, the model effectively captures
 151 the vertical profile (Fig. S1) and seasonality of U_{1060} (Fig. 1). Thus, while there may
 152 be discrepancies in certain aspects, the model remains a valuable tool for investigating the
 153 frequency of SSWs under varied boundary conditions as it outperforms many CMIP5/6
 154 models.

155 3.2 The impact of boundary conditions on SSWs

156 When topography is flattened in the model, the occurrence of SSWs in the NH nearly
 157 vanishes and so does the SSW asymmetry between the hemisphere (Table 1 FLAT), with
 158 only one SSW occurring during February in the NH. When the model is forced with
 159 symmetrized surface energy fluxes, which eliminates the ocean meridional overturning
 160 circulation, SSWs in the Northern Hemisphere decrease by half (Table 1 SYMS). When
 161 topography is flattened and symmetrized surface energy fluxes are applied (Table 1 F+S),
 162 no SSWs are observed throughout the 60-year simulation period in either hemisphere. The
 163 simulations suggest topography dominates the SSW hemispheric asymmetry with a smaller
 164 contribution from the ocean circulation. The results also indicate the boundary conditions
 165 interact nonlinearly.

3.3 The asymmetry of meridional eddy heat flux

To explain the changes in SSW frequency across our simulations, we next consider the meridional eddy heat flux, a representation of the upward propagation of planetary waves from the troposphere. The distribution of NH eddy heat flux at 100 hPa is positively skewed in ERA5 (Fig. 2a). The ALL simulation captures the ERA5 distribution well (Fig. 2b). The skewed distribution, particularly the long tail, implies that there is ample opportunity for internal variability to trigger a strong pulse of planetary wave forcing which can induce a SSW (Matsuno, 1971; Watt-Meyer & Kushner, 2018).

When the topography is flattened (Fig. 2c, e), the median value of the eddy heat flux distribution decreases, implying a reduced likelihood of upward wave propagation, consistent with the decrease in SSW frequency in the NH. However, symmetrizing the surface energy flux (Fig. 2d) exhibits a non-statistically significant impact on the wave forcing in the NH even though the SSW frequency decreases by 1/3 in the NH, consistent with the decrease in median value from 7.13 to 6.66 Km/s and 7% decrease in heat flux values exceeding 10Km/s. When topography is flattened and the surface energy fluxes are symmetrized the median value is once again significantly reduced suggesting topography is the dominant influence on the distribution.

In the SH, characterized by lower orographic features and a scarcity of SSWs, the meridional eddy heat flux distribution has a smaller median value and fewer extreme values (Fig. 2f, g). When topography is flattened the median value of the eddy heat flux distribution decrease (Fig. 2h) but it is weak and insignificant. Symmetrizing the surface energy flux also results in a decrease of the median of the eddy heat flux distribution (Fig. 2i, j). This is likely due to the predominance of oceanic areas in the SH, where applying symmetric surface energy flux average out the zonal differences in the surface energy flux, consequently weakening the stationary circulation.

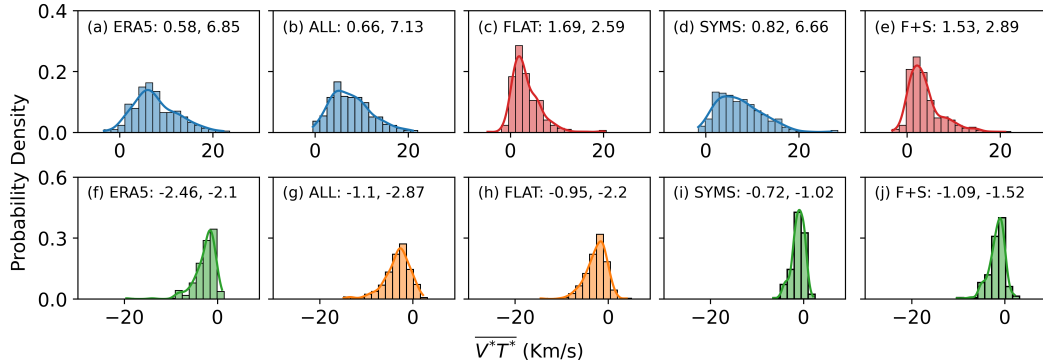


Figure 2. Distribution of monthly mean meridional eddy heat flux ($\overline{v^*T^*}$, Km s⁻¹) at 100 hPa averaged poleward of 45°N in SSW related season (Northern Hemisphere: Nov-Mar, Southern Hemisphere: May-Sep) in (a)(f) ERA5 and (b)(g) ALL, (c)(h) FLAT, (g)(i) SYMS, and (e)(j) F+S simulations. The top row is for Northern Hemisphere and the bottom row is for Southern Hemisphere. The value at the top of each panel are the skewness and median value of the distribution, respectively. Distributions that are significantly different from ALL (statistical significance at 95% level based on K-S test) have different colors.

To further investigate the impact of boundary conditions on the meridional eddy heat flux we examine its vertically-integrated spatial structure. The NH eddy heat flux in ERA5 (Fig. S2a) is large in the mid-latitude region (30°N-60°N) across various longitudes, especially around 120°E, which is captured by ALL (Fig. S2d). In contrast, the eddy heat

195 flux in the SH is small and doesn't exhibit significant longitudinal structure (Fig. S2b, e).
 196 Therefore, the simulation with topography reveals the most substantial asymmetry around
 197 120°E (Fig. 3a, b, d), aligning with the downstream location of the Tibetan Plateau.
 198 Averaged over the extratropics (20 to 90 degrees) the asymmetry is 40%, comparable with
 199 $\sim 50\%$ in ERA5 (Fig. 3f).

200 When topography is flattened, the hemispheric asymmetry significantly reduces across
 201 all longitudes (Fig. 3c, e). In particular, the extratropical asymmetry decreases from around
 202 40% to 3%, which is consistent with the decrease of eddy heat flux in the NH at 100 hPa
 203 (Fig. 2c, e). The impact of topography on the asymmetry of eddy heat flux is evident at
 204 850hPa (Fig. S3), 300 hPa (Fig. S4) and 100 hPa (Fig. S5), rather than being confined
 205 to a single level. Notably, the reduction in asymmetry is primarily due to the decrease in
 206 the NH, particularly around longitudes where significant topographical features exist (e.g.,
 207 120°E and 100°W), while the change in the SH is negligible.

208 In contrast, when surface energy fluxes are symmetrized the eddy heat flux asymmetry
 209 is not significantly reduced (Fig. 3d). Consistently the extratropical asymmetry is still
 210 37% (Fig. 3f). Symmetrizing decreases the meridional eddy heat flux in both hemispheres
 211 across all levels (Fig. S3h, S4h, S5h). Finally, when topography is flattened in the presence
 212 of symmetrized surface energy fluxes the meridional eddy heat flux asymmetry is once
 213 again negligible across all longitudes (Fig. 3e). Consistently, the extratropical asymmetry
 214 decreases to 7% (Fig. 3f). This shows that the boundary conditions interact non linearly
 215 in terms of their influence on the meridional eddy heat flux.

216 3.4 Understanding how topography affects the eddy heat flux asymmetry

217 The simulations show flattening exerts a dominant control on SSWs and the meridional
 218 eddy heat flux hemispheric asymmetry. Given the weak and negligible impact of topography
 219 on the distribution of eddy heat flux in the SH, we explore how topography affects the
 220 meridional eddy heat flux asymmetry, particularly focusing on its reduction in the NH. If
 221 v^* and T^* are represented using the complex exponential representation of a Fourier series,
 222 their covariance $\overline{v^*T^*}$ can be written as

$$\overline{v^*T^*} = A_v A_T e^{i(\theta_v - \theta_T)} \quad (1)$$

223 where A_v and A_T are the amplitude of v^* and T^* , θ_v and θ_t are the phase of v^* and T^* .

224 Consequently, the decrease in eddy heat flux ($\overline{v^*T^*}$) when topography is flattened might
 225 arise from various factors, including a decline in amplitude of eddy meridional wind (v^*)
 226 and/or eddy temperature (T^*), as well as a increase in the difference between their phases,
 227 namely the two variables becoming out of phase.

228 Fig. 4 shows the probability distribution of the amplitude, and phase difference of
 229 monthly mean eddy meridional wind and eddy temperature at 100 hPa and 60°N across
 230 the climate model simulations following Watt-Meyer and Kushner (2018). Flattenning
 231 topography results in a decrease of over 30% in the median value of the wave-1 amplitude
 232 for both eddy meridional wind (Fig. 4a) and eddy temperature (Fig. 4b). Furthermore,
 233 the phase difference between the two variables becomes slightly larger when topography is
 234 removed (Fig. 4c).

235 For the wave-2 component, the mode of the amplitude distributions decreases by over
 236 20% when topography is removed (Fig. 4d, e) while the change in the median value is
 237 less significant compared to the wave-1 component. In contrast, the eddy meridional wind
 238 and temperature become more out of phase in the absence of topography (Fig. 4f). The
 239 phase difference increases by approximately 40% following flattening topography, thereby
 240 contributing to the decline in eddy heat flux in the Northern Hemisphere. Moving towards
 241 larger wavenumber components, a reduction in the amplitude of eddy temperature (Fig.
 242 S6b, e) is evident. However, variations in other components remain relatively modest.

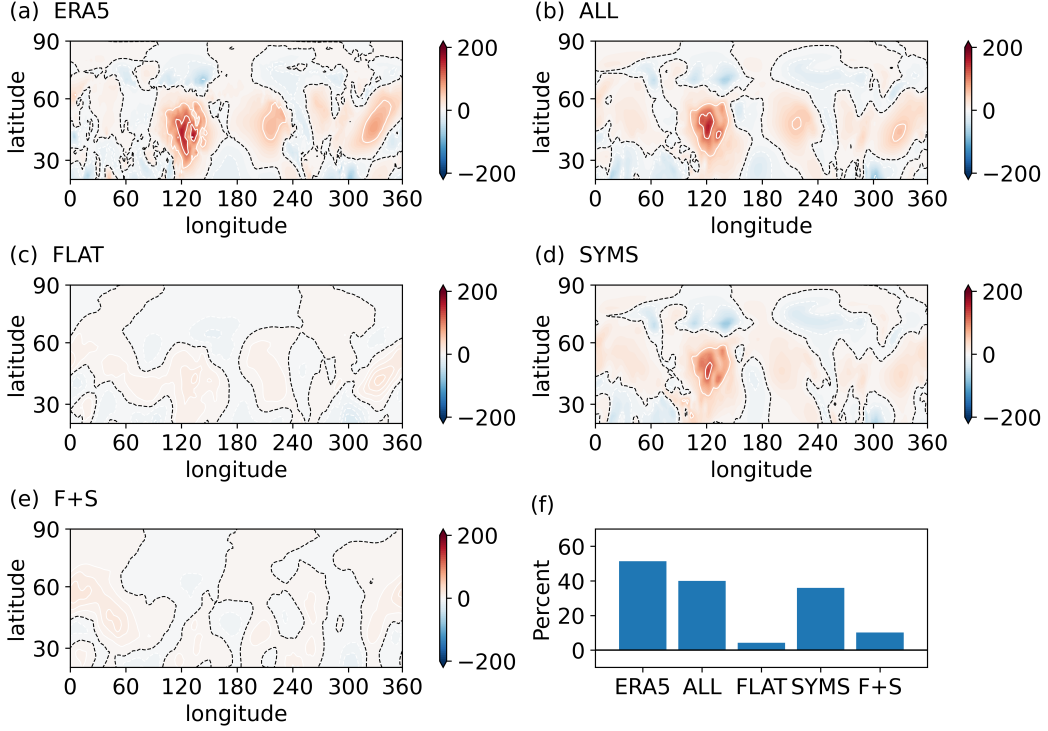


Figure 3. Difference of the vertically integrated monthly mean meridional eddy heat flux ($\overline{v^*T^*}$, K m s^{-1}) between Northern and Southern Hemispheres in SSW related season (NH: Nov-Mar, SH: May-Sep) in (a) ERA5, (b) ALL, (c) FLAT, (d) SYMS and (e) F+S simulations. The dashed black lines indicates where $\overline{v^*T^*}$ is equal to 0 MJ m^{-2} . (f) Percentage difference of zonal-mean, vertically integrated stationary eddy heat flux ($\overline{v^*T^*}$, K m s^{-1}) (difference of the absolute value of Northern and Southern Hemisphere divided by Northern Hemisphere) averaged over poleward of 20° across the simulations.

243 Overall, the reduction in wave-1 heat flux is due to a reduction in the amplitude of v^* ,
 244 T^* , and an increase in the phase difference, while the reduction in wave-2 median heat flux
 245 is driven mainly by the phase difference.

246 4 Discussion

247 In this study, we used climate model simulations to quantify the impact of boundary
 248 conditions on the hemispheric asymmetry of SSWs. Our approach aligns with prior
 249 studies that used climate models to understand the impact of boundary conditions on the
 250 hemispheric asymmetry of atmospheric features (Manabe & Terpstra, 1974; Frierson et
 251 al., 2013; Shaw et al., 2022). More specifically we quantified the impact of topography by
 252 flattening it, and the impact of the ocean meridional overturning circulation by symmetrizing
 253 the surface energy fluxes in the slab ocean (Stevens et al., 2013).

254 Our goal was to answer the two questions posed in the Introduction. Namely (1) What
 255 are the relative contributions of boundary conditions, including topography and the ocean
 256 meridional overturning circulation, on the hemispheric asymmetry of SSWs? (2) Through
 257 what mechanisms do boundary conditions affect stratospheric variability?

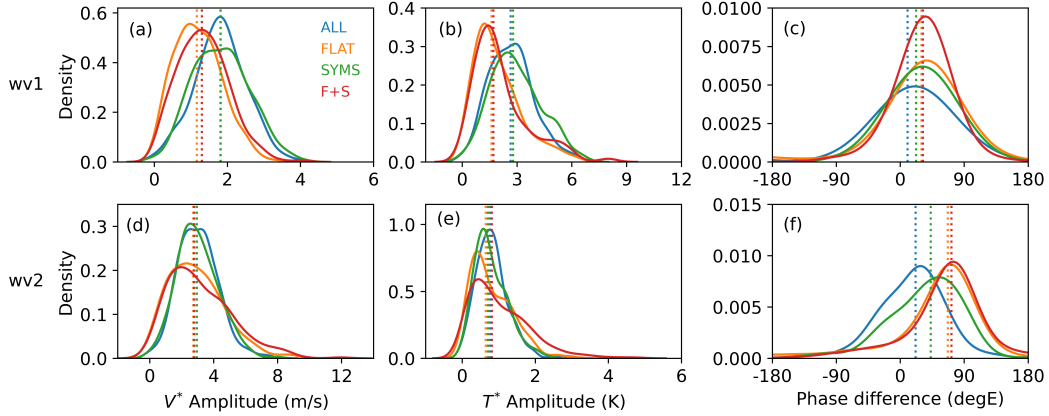


Figure 4. Probability distribution of the amplitude of monthly mean eddy meridional wind (v^* , m s^{-1}) (the first column) and monthly mean eddy temperature (T^* , K) (the second column), and the phase difference between the two variables (the third column) in the NH for (a)-(c) wave-1 and (d)-(f) wave-2 component at 60°N and 100 hPa in SSW related season (Northern Hemisphere: Nov-Mar) for ALL (blue), FLAT (orange), SYMS (green), and F+S (red) simulations. The dotted lines represents the median value for each distribution.

258 The answer to the first question is that topography dominates the hemispheric
 259 asymmetry of SSWs while the asymmetric surface energy fluxes plays a smaller role in the
 260 presence of topography. Topography essentially eliminates SSWs in the NH and eliminates
 261 the hemispheric asymmetry. Symmetrizing surface energy fluxes only reduces NH SSWs by
 262 1/3. Notably, the impact of topography on the asymmetry percentage of eddy heat flux is
 263 substantial, exceeding 35%, with non-additive contributions from various boundary forcings
 264 indicating nonlinear interactions among them. Although our results demonstrate that the
 265 boundary conditions interact nonlinearly in terms of their impact on SSWs, it is clear that
 266 topography is the more significant factor.

267 The answer to the second question is that topography affects stratospheric variability by
 268 increasing the amplitude of eddy temperature and meridional winds, and decreasing their
 269 phase difference. Specifically, removal of topography results in a decrease in the median
 270 value of the amplitude for both eddy meridional wind and eddy temperature, particularly
 271 for wave number 1. This reduction is accompanied by an increase in the phase difference
 272 between the two variables, namely they becomes more out of phase with each other. These
 273 changes in both amplitude and phase induced by topography lead to a regional increase in
 274 eddy heat flux, especially over Eurasia, which indicates upward propagation of planetary
 275 waves into the stratosphere, thereby disturbing the polar vortex and causing more SSWs.

276 Our results are consistent with previous work that demonstrated topography
 277 significantly affects stationary wave features (Manabe & Terpstra, 1974; Held, 1983;
 278 Garfinkel et al., 2020). It is commonly assumed that both topography and land-ocean
 279 contrast contribute to the hemispheric asymmetry of SSWs and eddy heat flux. However,
 280 our analysis shows topography is the dominant factor.

281 While our simulations do not specifically isolate the impact of thermal forcing from
 282 land-sea contrast, our result suggest that the hemispheric asymmetry of SSWs are minimal
 283 with flattened topography even in the presence of land-sea contrast. Furthermore the
 284 fact that the eddy heat flux asymmetry in the simulation with flattened topography is
 285 small strongly suggests that topography exerts a more substantial influence than land-
 286 sea contrast. By flattening the topography, the contributions of both the topography and

287 nonlinear interaction between topographic and thermal forcings are excluded, leaving only
 288 the minor contribution from thermal forcing. Reproducing these results in other climate
 289 models is important to ensure their robustness.

290 5 Data Availability Statement

291 The data analyzed in this study is available through Shaw et al., 2022.

292 References

- 293 Afargan-Gerstman, H., & Domeisen, D. I. (2020). Pacific modulation of the north atlantic
 294 storm track response to sudden stratospheric warming events. *Geophysical Research*
 295 *Letters*, *47*(2), e2019GL085007.
- 296 Allen, D. R., Bevilacqua, R. M., Nedoluha, G. E., Randall, C. E., & Manney, G. L.
 297 (2003). Unusual stratospheric transport and mixing during the 2002 antarctic winter.
 298 *Geophysical Research Letters*, *30*(12).
- 299 Allen, D. R., Coy, L., Eckermann, S. D., McCormack, J. P., Manney, G. L., Hogan, T. F.,
 300 & Kim, Y.-J. (2006). Nogaps-alpha simulations of the 2002 southern hemisphere
 301 stratospheric major warming. *Monthly weather review*, *134*(2), 498–518.
- 302 Baldwin, M. P., Ayarzagüena, B., Birner, T., Butchart, N., Butler, A. H., Charlton-Perez,
 303 A. J., ... others (2021). Sudden stratospheric warmings. *Reviews of Geophysics*,
 304 *59*(1), e2020RG000708.
- 305 Baldwin, M. P., & Dunkerton, T. J. (1999). Propagation of the arctic oscillation from
 306 the stratosphere to the troposphere. *Journal of Geophysical Research: Atmospheres*,
 307 *104*(D24), 30937–30946.
- 308 Baldwin, M. P., & Dunkerton, T. J. (2001). Stratospheric harbingers of anomalous weather
 309 regimes. *Science*, *294*(5542), 581–584.
- 310 Butler, A. H., Seidel, D. J., Hardiman, S. C., Butchart, N., Birner, T., & Match, A. (2015).
 311 t. *Bulletin of the American Meteorological Society*, *96*(11), 1913–1928.
- 312 Charlton, A. J., & Polvani, L. M. (2007). A new look at stratospheric sudden warmings.
 313 part i: Climatology and modeling benchmarks. *Journal of climate*, *20*(3), 449–469.
- 314 Charney, J. G., & Eliassen, A. (1949). A numerical method for predicting the perturbations
 315 of the middle latitude westerlies. *Tellus*, *1*(2), 38–54.
- 316 Cohen, J., & Jones, J. (2011). Tropospheric precursors and stratospheric warmings. *Journal*
 317 *of climate*, *24*(24), 6562–6572.
- 318 Dunn-Sigouin, E., & Shaw, T. (2018). Dynamics of extreme stratospheric negative heat flux
 319 events in an idealized model. *Journal of the Atmospheric Sciences*, *75*(10), 3521–3540.
- 320 Dunn-Sigouin, E., & Shaw, T. (2020). Dynamics of anomalous stratospheric eddy heat flux
 321 events in an idealized model. *Journal of the Atmospheric Sciences*, *77*(6), 2187–2202.
- 322 Dunn-Sigouin, E., & Shaw, T. A. (2015). Comparing and contrasting extreme stratospheric
 323 events, including their coupling to the tropospheric circulation. *Journal of Geophysical*
 324 *Research: Atmospheres*, *120*(4), 1374–1390.
- 325 Frierson, D. M., Hwang, Y.-T., Fučkar, N. S., Seager, R., Kang, S. M., Donohoe, A., ...
 326 Battisti, D. S. (2013). Contribution of ocean overturning circulation to tropical rainfall
 327 peak in the northern hemisphere. *Nature Geoscience*, *6*(11), 940–944.
- 328 Garfinkel, C. I., White, I., Gerber, E. P., Jucker, M., & Erez, M. (2020). The building blocks
 329 of northern hemisphere wintertime stationary waves. *Journal of Climate*, *33*(13),
 330 5611–5633.
- 331 Gerber, E. P., & Polvani, L. M. (2009). Stratosphere–troposphere coupling in a relatively
 332 simple agcm: The importance of stratospheric variability. *Journal of Climate*, *22*(8),
 333 1920–1933.
- 334 Held, I. M. (1983). Stationary and quasi-stationary eddies in the extratropical troposphere:
 335 Theory. *Large-scale dynamical processes in the atmosphere*, *127*, 168.
- 336 Held, I. M., Ting, M., & Wang, H. (2002). Northern winter stationary waves: Theory and
 337 modeling. *Journal of climate*, *15*(16), 2125–2144.

- 338 Hendon, H. H., Thompson, D., Lim, E.-P., Butler, A. H., Newman, P. A., Coy, L., & Scaife,
339 A. (2019). Rare forecasted climate event under way in the southern hemisphere.
340 *Nature*, *573*(7775), 495–496.
- 341 Hersbach, H., Bell, B., Berrisford, P., Hirahara, S., Horányi, A., Muñoz-Sabater, J.,
342 ... others (2020). The era5 global reanalysis. *Quarterly Journal of the Royal
343 Meteorological Society*, *146*(730), 1999–2049.
- 344 Jucker, M., & Reichler, T. (2023). Life cycle of major sudden stratospheric warmings in
345 the southern hemisphere from a multimillennial gcm simulation. *Journal of Climate*,
346 *36*(2), 643–661.
- 347 Krüger, K., Naujokat, B., & Labitzke, K. (2005). The unusual midwinter warming in
348 the southern hemisphere stratosphere 2002: A comparison to northern hemisphere
349 phenomena. *Journal of the atmospheric sciences*, *62*(3), 603–613.
- 350 Lehtonen, I., & Karpechko, A. Y. (2016). Observed and modeled tropospheric cold anomalies
351 associated with sudden stratospheric warmings. *Journal of Geophysical Research:
352 Atmospheres*, *121*(4), 1591–1610.
- 353 Lim, E.-P., Hendon, H. H., Boschat, G., Hudson, D., Thompson, D. W., Dowdy, A. J., &
354 Arblaster, J. M. (2019). Australian hot and dry extremes induced by weakenings of
355 the stratospheric polar vortex. *Nature Geoscience*, *12*(11), 896–901.
- 356 Lindgren, E., Sheshadri, A., & Plumb, R. (2018). Sudden stratospheric warming formation
357 in an idealized general circulation model using three types of tropospheric forcing.
358 *Journal of Geophysical Research: Atmospheres*, *123*(18), 10,125–10,139.
- 359 Manabe, S., & Terpstra, T. B. (1974). The effects of mountains on the general circulation
360 of the atmosphere as identified by numerical experiments. *Journal of Atmospheric
361 Sciences*, *31*(1), 3–42.
- 362 Matsuno, T. (1971). A dynamical model of the stratospheric sudden warming. *Journal of
363 Atmospheric Sciences*, *28*(8), 1479–1494.
- 364 Plumb, R. A. (1989). On the seasonal cycle of stratospheric planetary waves. *Pure and
365 applied geophysics*, *130*, 233–242.
- 366 Polvani, L. M., & Waugh, D. W. (2004). Upward wave activity flux as a precursor to extreme
367 stratospheric events and subsequent anomalous surface weather regimes. *Journal of
368 Climate*, *17*(18), 3548–3554.
- 369 Rao, J., & Garfinkel, C. I. (2021). Cmp5/6 models project little change in the statistical
370 characteristics of sudden stratospheric warmings in the 21st century. *Environmental
371 Research Letters*, *16*(3), 034024.
- 372 Rao, J., Garfinkel, C. I., White, I. P., & Schwartz, C. (2020). The southern hemisphere
373 minor sudden stratospheric warming in september 2019 and its predictions in s2s
374 models. *Journal of Geophysical Research: Atmospheres*, *125*(14), e2020JD032723.
- 375 Scaife, A. A., Woollings, T., Knight, J., Martin, G., & Hinton, T. (2010). Atmospheric
376 blocking and mean biases in climate models. *Journal of Climate*, *23*(23), 6143–6152.
- 377 Scinocca, J., & Haynes, P. (1998). Dynamical forcing of stratospheric planetary waves by
378 tropospheric baroclinic eddies. *Journal of the Atmospheric Sciences*, *55*(14), 2361–
379 2392.
- 380 Shaw, T. A., Miyawaki, O., & Donohoe, A. (2022). Stormier southern hemisphere induced by
381 topography and ocean circulation. *Proceedings of the National Academy of Sciences*,
382 *119*(50), e2123512119.
- 383 Shaw, T. A., & Perlwitz, J. (2013). The life cycle of northern hemisphere downward
384 wave coupling between the stratosphere and troposphere. *Journal of climate*, *26*(5),
385 1745–1763.
- 386 Shaw, T. A., & Perlwitz, J. (2014). On the control of the residual circulation and
387 stratospheric temperatures in the arctic by planetary wave coupling. *Journal of the
388 Atmospheric Sciences*, *71*(1), 195–206.
- 389 Sheshadri, A., Plumb, R. A., & Gerber, E. P. (2015). Seasonal variability of the polar
390 stratospheric vortex in an idealized agcm with varying tropospheric wave forcing.
391 *Journal of the Atmospheric Sciences*, *72*(6), 2248–2266.
- 392 Simmons, A., Hortal, M., Kelly, G., McNally, A., Untch, A., & Uppala, S. (2005). Ecmwf

- 393 analyses and forecasts of stratospheric winter polar vortex breakup: September 2002
394 in the southern hemisphere and related events. *Journal of the Atmospheric Sciences*,
395 *62*(3), 668–689.
- 396 Sjoberg, J. P., & Birner, T. (2012). Transient tropospheric forcing of sudden stratospheric
397 warmings. *Journal of the Atmospheric Sciences*, *69*(11), 3420–3432.
- 398 Sjoberg, J. P., & Birner, T. (2014). Stratospheric wave–mean flow feedbacks and sudden
399 stratospheric warmings in a simple model forced by upward wave activity flux. *Journal*
400 *of the Atmospheric Sciences*, *71*(11), 4055–4071.
- 401 Smagorinsky, J. (1953). The dynamical influence of large-scale heat sources and sinks on
402 the quasi-stationary mean motions of the atmosphere. *Quarterly Journal of the Royal*
403 *Meteorological Society*, *79*(341), 342–366.
- 404 Stevens, B., Giorgetta, M., Esch, M., Mauritsen, T., Crueger, T., Rast, S., ... others
405 (2013). Atmospheric component of the mpi-m earth system model: Echam6. *Journal*
406 *of Advances in Modeling Earth Systems*, *5*(2), 146–172.
- 407 Taguchi, M., & Yoden, S. (2002). Internal interannual variability of the
408 troposphere–stratosphere coupled system in a simple global circulation model. part
409 i: Parameter sweep experiment. *Journal of the Atmospheric Sciences*, *59*(21), 3021–
410 3036.
- 411 Thompson, D. W., Baldwin, M. P., & Solomon, S. (2005). Stratosphere–troposphere
412 coupling in the southern hemisphere. *Journal of the atmospheric sciences*, *62*(3),
413 708–715.
- 414 Varotsos, C. (2002). The southern hemisphere ozone hole split in 2002. *Environmental*
415 *Science and Pollution Research*, *9*, 375–376.
- 416 Watt-Meyer, O., & Kushner, P. J. (2018). Why are temperature and upward wave activity
417 flux positively skewed in the polar stratosphere? *Journal of Climate*, *31*(1), 115–130.
- 418 Wu, Z., & Reichler, T. (2020). Variations in the frequency of stratospheric sudden warmings
419 in cmip5 and cmip6 and possible causes. *Journal of Climate*, *33*(23), 10305–10320.
- 420 Yamazaki, Y., Matthias, V., Miyoshi, Y., Stolle, C., Siddiqui, T., Kervalishvili, G., ... others
421 (2020). September 2019 antarctic sudden stratospheric warming: Quasi-6-day wave
422 burst and ionospheric effects. *Geophysical Research Letters*, *47*(1), e2019GL086577.